The Astrophysical Journal, 730:57 (9pp), 2011 March 20 doi:10.1088/0004-637X/730/1/57

RADIO EVIDENCE OF BREAK-OUT RECONNECTION?

H. Aurass[1], G. Mann[1], P. Zlobec[2], and M. Karlický[3]
[1] Astrophysikalisches Institut Potsdam, An der Sternwarte 16, D-14482 Potsdam, Germany
[2] INAF-Osservatorio Astronomico di Trieste, via G.B. Tiepolo 11, I-34143 Trieste, Italy
[3] Astronomical Institute of the Czech Academy of Sciences, Fričova 298, CZ-25165 Ondřejov, Czech Republic
Received 2010 November 2; accepted 2011 January 21; published 2011 March 3

ABSTRACT

We reconsider the 2003 October 28 X17 flare/coronal mass ejection (CME), studying the five minutes immediately before the impulsive flare phase (not discussed in previous work). To this aim we examine complementary dynamic radio spectrograms, single frequency polarimeter records, radio images, space-based longitudinal field magnetograms, and ultraviolet images. We find widely distributed faint and narrowband meter wave radio sources located outside active regions but associated with the boundaries of magnetic flux connectivity cells, inferred from the potential extrapolation of the observed photospheric longitudinal field as a model for coronal magnetic field structures. The meter wave radio sources occur during the initial decimeter wave effects, which are well known to be associated with filament destabilization in the flaring active region (here NOAA 10486). Antiochos et al. predict in their break-out model for CME initiation that "... huge phenomena ... may be controlled by detailed plasma processes that occur in relatively tiny regions." They suggest that the expected faint energy release "... on long field lines far away from any neutral line ... may be detectable in radio/microwave emission from nonthermal particles..." In this paper, we describe meter wave sources whose properties correctly coincide with the quoted predictions of the break-out reconnection model of the CME initiation.

Key words: Sun: corona – Sun: coronal mass ejections (CMEs) – Sun: flares – Sun: magnetic topology – Sun: radio radiation

1. INTRODUCTION

Coronal mass ejections (CMEs) and flares are two consequences of magnetic energy release in the solar (and therefore also magnetized stellar) corona(e). The initial stages of both, frequently interrelated processes are the most difficult to observe. However, understanding this initiation is the key to understanding space weather disturbances and to developing early-warning methods in the Sun–Earth system.

In several papers, Antiochos and colleagues (Antiochos et al. 1999, 2002; MacNeice et al. 2004; Lynch et al. 2008) propose the "magnetic break-out model" of CMEs. They consider magnetic field relaxation by reconnection at separatrices (Somov 1986, 2000) as follows. Large-scale magnetic field structures, above a stressed magnetic arcade, undergo reconnection in a quasi-steady way, implying a minor energy release when compared with that of the consequent flare or CME. Priest & Démoulin (1995) and Démoulin et al. (1996) introduced the concept of quasi-separatrix-layers (QSLs), thin volumes where field connectivity changes drastically and reconnection can occur.

By reducing the tension in structures above the preflare configuration, the structural changes by reconnection lead to the release of the twist and shear of the preflare filament. It can start its fast rise together with the occurrence of the other well-known flare signatures, and a CME can be formed in the surrounding corona. This model differs from two other approaches: the flux rope instability model (Chen 1989; Kliem & Török 2006) and the classical catastrophe model based on the CSHKP model (named for its promoters Carmichael, Sturrock, Hirayama, Kopp, and Pneumann) for eruptive—or two ribbon—flares, e.g., Priest & Forbes (2000). Namely, it predicts early observable consequences of CME initiation, which are signs of reconnection at QSLs somewhere along extended coronal field lines. The associated radio emission of thereby accelerated electrons brightens far away from active regions at least several minutes before it is possible to identify the CME in EUV and (still later) in coronagraph images. The expected radio sources can occur without related effects in other spectral ranges.

The 2003 October 28 halo-CME and X17 flare in NOAA 10486 (see Figure 1 for a map of the flaring active region and its surroundings) has already been analyzed in a number of papers. Pick et al. (2005) were the first to show expanding belts of radio emission at 432, 410.5, and 327 MHz during the impulsive phase centered around the flaring active region (11:02:42–11:10 UT) and to indicate radio emission from the expanding CME bubble. Kiener et al. (2006) presented data about the strongest emission of >10 MeV electrons in the same time interval where Aurass et al. (2006) found radio spectral signatures for a standing coronal shock wave interpreted as radiation of the reconnection outflow termination shock (11:02:40–11:03:40). Hurford et al. (2006) confirmed *RHESSI*[4] observations of a systematic spatial shift between hard X-ray (HXR) and γ-ray sources. Several authors (e.g., Klassen et al. 2005) analyzed the particle data of the associated ground-level event. Mandrini et al. (2006) studied the evolution of a small event preceding the X-class flare by 1 hr. They modeled the coronal magnetic field in and next to AR 10486 and interpreted the observation of four 1600 Å brightenings as the result of magnetic reconnection at QSLs. In their view, this was evidence of the break-out model for the CME initiation. The events preceding the X-class flare occurred in the trailing part of AR 10486 and are coupled with the rise of two narrow CMEs above the east limb (see Table 1 for a synopsis). Trottet et al. (2008) discussed submillimeter observations of the event and found impulsive and long-duration components of synchrotron radiation.

The main flare starts between 10:58:30 UT (μ-wave/dm-wave emission) and 11:02:47 UT (signaled by strong broadband

[4] The *Ramaty High Energy Solar Spectroscopic Imager*; Lin et al. (2002).

Table 1
2003 October 28 AR 10486

Phenomenon	Time (UT)	Remarks
CME PA22	8:50–9:04 onset	$v = 853$ km s^{-1}
CME PA147	≈10:35 onset	$v = 1054$ km s^{-1}
Halo-CME	11:00 onset	$v = 2495$ km s^{-1}
Preflare/CME	10:05–10:59:25	EIT/*TRACE*/*RHESSI*
Signatures		East of AR 10486
Radio		
	Drifting CME cont.	10:34 reaching $f < 40$ MHz
	correlated long meter /	Max. 10:36 (Figure 3 of Pick et al. 2005)
	decimeter flux	(as, e.g., Reiner et al. 2000)
SXR	rise 10:59:30	(time derivative)
Radio		
New source	10:58:30	Source A (250–<200 MHz);
	rise in microwaves	
Flare in AR 10486	10:58:30–11:01:24	2–1 GHz drift. puls. struct. (DPS)
New source	11:01:10	Source B (250–<200 MHz)
New source	11:01:30–11:02:20	±327 MHz, P1, $T \approx 1$ s, pol.≈70 R
	11:02:19–11:02:25	3 zebra stripes ±1420 MHz, pol.≈12 R
New sources	11:02:24–11:02:33	±236 MHz, P2, $T \approx 0.5$ s, pol.≈38···20 R
Eruption	>11 : 02 : 30	large burst and termin. shock (radio) +
		HXR and γ-ray sources and motion in 284 Å
Reappearance at the	11:13–11:21	pol. 4% R (till 11:13), 4% L (11:14:10)
early 327 MHz site		64% L after cutoff(11:25)
		pol.sense reversal!!

Notes. ±236 MHz (e.g.) means that an effect was observed with its spectrum being broader but <100 MHz. All polarization values are determined above the background level.

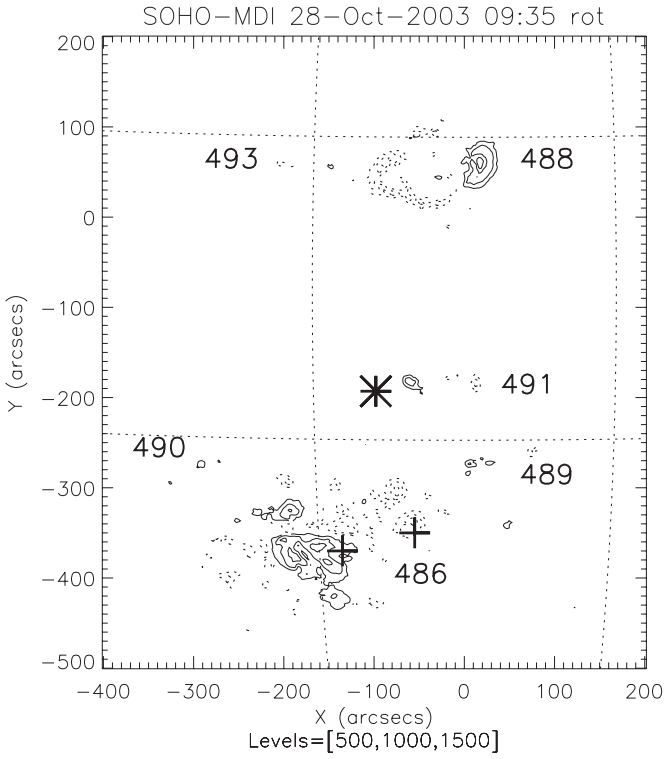

Figure 1. *SOHO*-MDI longitudinal field of AR 10486 and surroundings. The isoline levels are given in the subtitle (1 Gauss = 10^{-4} Tesla). We show the preflare magnetogram (09:35 UT) rotated to 11:02:30 UT (impulsive phase). North is top and east is left. The active region numbers are NOAA 10xxx. The plus signs are the *RHESSI* HXR source centroid positions (as in Aurass et al. 2006); the asterisk is placed near the end point of converging flux cell boundaries according to Figure 4 in Aurass et al. (2007). This low field region is magnetically connected with ARs 486, 491, and 488 (ibid).

radio emission, a southwest motion of a hot part of a filament seen in EUV, and Hα flare ribbons brightening and expanding). The back extrapolation of the halo-CME that occurs along with this flare indicates the same time interval for the onset of the CME motion.

In different archives, we found more data about this early stage of the CME and flare development. They are presented in Section 2 and considered here under the aspect of the prediction by Antiochos et al. (1999) as well as the magnetic field analysis of Mandrini et al. (2006) and Aurass et al. (2006, 2007; Section 3). We conclude in Section 4 that radio sources with properties as predicted by Antiochos et al. (1999) for the magnetic break-out model of CMEs can be well observed during the analyzed event.

2. OBSERVATIONS

For the description of the spectrographs, we refer to Mann et al. (1992) and Jiřička et al. (1993) for the Astrophysical Institute Potsdam (AIP, 40–800 MHz) and Astronomical Observatory Ondřejov (AOO, 0.8–4 GHz). Kerdraon & Delouis (1997) give a description of the Nançay Multifrequency Radioheliograph (NRH) of the Observatory of Paris–Meudon, France. In this work, we use radio images only at 327 and 236.6 MHz. The single frequency high time resolution polarimeters of the Astronomical Observatory of Trieste (INAF-OAT) are described at http://radiosun.ts.astro.it. The data from the *Solar and Heliospheric Observatory* (*SOHO*; Fleck et al. 1995) and *Transition Region and Coronal Explorer* (*TRACE*; Handy et al. 1999) are important for this work. We use magnetic field data in spherical coordinates as provided by the potential field source surface (pfss) branch in the solar software (Schrijver & DeRosa 2003). For CME data, we refer to the listing initiated by N. Gopalswamy; the CME onset

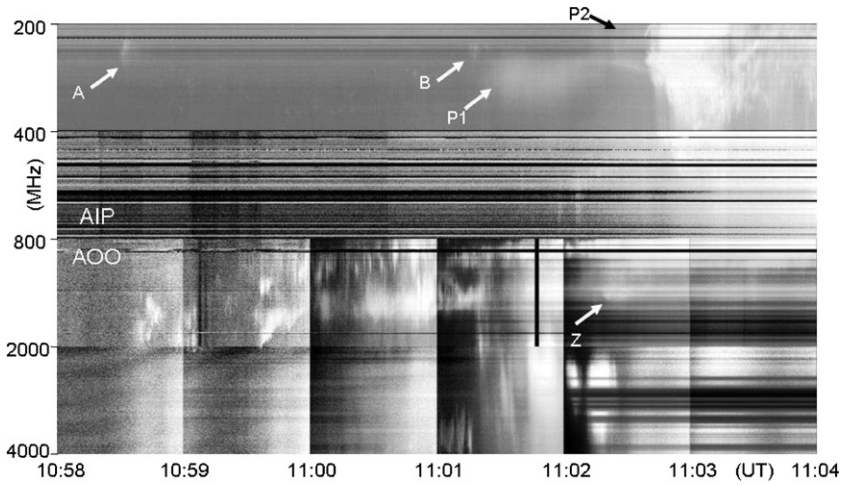

Figure 2. Composed spectrum (Astrophysical Institute Potsdam and Astronomical Observatory Ondřejov) of the X17 flare 2003 October 28, 10:58–11:04 UT, 0.2–4 GHz. The color table: white is large flux and black is background. The time-parallel lines are terrestrial transmitters. AOO spectra are contrast-enhanced in 1 minute steps. The brightness in the intervals is not comparable. Features P1 and P2 are <100 MHz wide pulsations (see Figure 3). Features A and B are faint drift bursts and *Z* denotes a 6 s interval with three zebra stripes at ≈1420 MHz.

times result from the linear back extrapolation given there (http://cdaw.gsfc.nasa.gov/CME_list/index.html).

The start of the event is extraordinarily well observed because two narrowband radio features of special interest are situated in the dynamic radio spectrum around NRH imaging and OAT polarimeter frequencies. Figure 2 is a composed spectrogram from AIP and AOO showing the strong and broadband radiation enhancements at 11:02:47 UT. The time thereafter is discussed by Pick et al. (2005), Aurass et al. (2006, 2007), and other authors. For the moment, we focus our attention on the earlier time interval (10:58:30–11:02:30 UT) which is after the time considered by Mandrini et al. (2006).

In this time interval, Figure 2 shows faint pulsation patches with a bandwidth <100 MHz, around 327 MHz and 237 MHz, in time sequence. The associated polarimeter records in Figure 3 show that the signals are right-handed (R-) polarized, with fast pulsations overlaid in the R channel only. The pulsating meter wave emissions are denoted as P1 and P2 in Figure 2. Figure 3 shows that P1 (327 MHz) is superposed on an almost symmetric smooth rise and fall of intensity. The simultaneous 237 MHz OAT record reveals a sequence of pulses (quasi-period of ≈20 s). Its background starts to grow toward the eruption, with the faster (P2) pulsations superimposed after the fadeout of P1 in the 327 MHz record.

The spectral analysis of the short-period fluctuations shows that the 327 MHz pulsation (P1) has a period of ≈1.1 ± 0.2 s (see the power spectra in Figure 3(b)). In contrast, the 237 MHz pulsation P2 is faster—we obtained a period of 0.48 ± 0.05 s. That means that, barring a correspondence by chance, the fluctuation P2 may well be a harmonic of P1. We note that the observed frequency dependence of the pulsation period is anomalous. Regularly, longer time scales are expected at lower frequencies (see also Magdalenič et al. 2002). This contrast suggests two physically different sources of P1 and P2. The oscillations of radio emission in the remote source P2 are twice as fast as in P1 in approaching the impulsive energy release in AR 10486. The underlying pulses with about 20 s repetition rate come from slightly different sites of the considered area of distributed radio sources.

In the 0.8–4 GHz range, the spectrum reveals a pattern of drifting pulsating structures (DPS) from 10:58:30–11:01:20 UT. At the P1 onset at 327 MHz the decimeter emission bandwidth

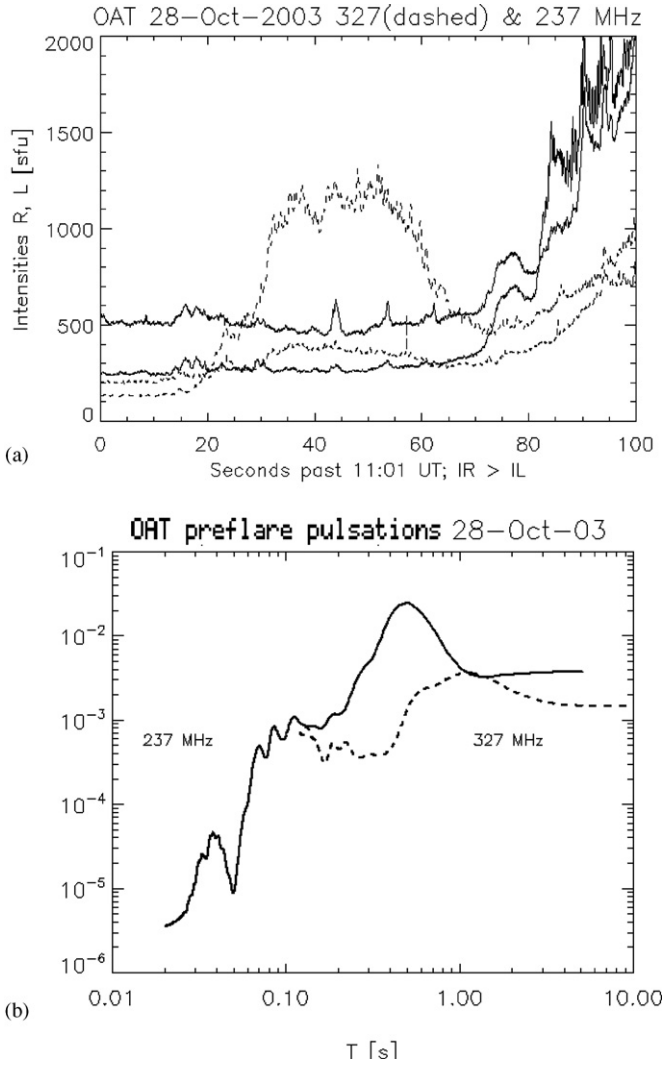

Figure 3. OAT 237 MHz and 327 MHz (dashed) polarimeter records. (a) The flux curves demonstrating the circularly polarized (right-handed, R) emission of P1 and P2 in Figure 2. At 237 MHz an ≈20 s quasi-period is evident and superposed by much faster fluctuations. (b) The power spectra of P1 and P2. The *y*-axis is scaled in arbitrary units. The fluctuation period changes from about 1 s (P1) to 0.5 s (P2) before the eruption.

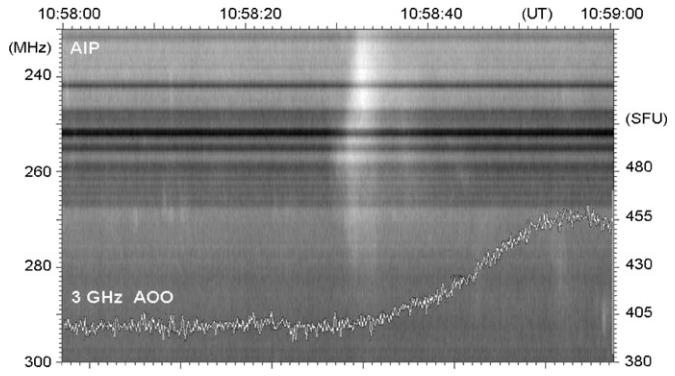

Figure 4. Enlarged spectral signature of radio source A (AIP, left scale: frequency (MHz)) with the overplotted 3 GHz radiation flux (AOO, right scale, in solar flux units, 10^{-22} W Hz^{-1} m^{-2}).

broadens suddenly over the whole range of AOO data. We also notice a faint trace of emission between the DPS and the impulsive onset at meter waves drifting from 800 to 400 MHz in the interval 11:01:40–11:02:40 UT.

For our further discussion, it is important to consider two faint drift bursts (arrows A and B in Figure 2). Feature A occurs with the beginning of the decimeter emission at 10:58:30 UT. We have enlarged the corresponding part of the radio spectrum and overplotted the AOO 3 GHz single frequency record (Figure 4). This figure confirms that the very first narrowband meter wave source in the analyzed preflare time interval occurs simultaneously with the onset of the preflare rise of the 3 GHz radio flux curve despite the wide frequency spacing of both phenomena. This recalls the work of Reiner et al. (2000) concerning the sometimes remarkable correlation between the decimeter and the hectometer radio flux—the one surely associated with the flare process in an active region near the transition to the chromosphere, the other escaping in coronal heights far above 1 $R_\odot$. Still more interesting is the viewpoint that source A, starting at 258 MHz, is excited by electron beams as suggested by its pattern in the dynamic radio spectrum. In this case, the spectrum means that one beam propagates from the acceleration region (at a plasma frequency of 258 MHz) with almost no time delay toward higher densities, the other with a "type III burst-like" time delay toward lower densities. This can be understood to mean the radiating electrons are not accelerated in a loop structure with the density stratification known from, e.g., type U or reverse drift bursts. We argue that this radio signature is formed if one electron beam penetrates into the denser layers of a magnetic neutral sheet (inside a QSL) with an extremely short density height scale (propagating a short path only, thus showing no frequency drift), and another escapes into the surrounding space along extended coronal magnetic field lines with the typical coronal density scale height.

Feature B occurs simultaneously with the onset of the pulsation patch P1 in the meter wave range and the sudden spectral broadening of varying dm/μ-wave radiation. The three distinct zebra stripes[5] are a remarkable detail of the dm wave spectrum. They occur at 1420 MHz only in the transition time from meter wave source P1 to P2 (11:02:19–11:02:25 UT). The stripe frequency spacing is $\leqslant$200 MHz (see Figure 5(b)).

The composed dynamic radio spectrum demonstrates that there is synchronism between radio signatures widely spaced in frequency. No imaging data are available above 432 MHz (the largest NRH observing frequency). This means that we must speculate about the source site of the decimetric emission that starts together with source A. From earlier work (e.g., Barta et al. 2008) we know that such lanes with superposed DPS are a typical signature of the flare start. Karlický (2004) showed that fragmentation of energy release during the early stage of the evolution of the flare current sheet should induce such radio features. Based on this experience, we assume that the emission above 800 MHz reflects flare current sheet formation and dynamics. The dm source sites are situated underneath and around the erupting filament in AR 10486.

With the m-wave bursts we are in a better situation to use the imaging observations of the NRH (Kerdraon & DeLouis 1997). Figure 5(a) shows the source sites of P1 (at 327 MHz) and P2 (at

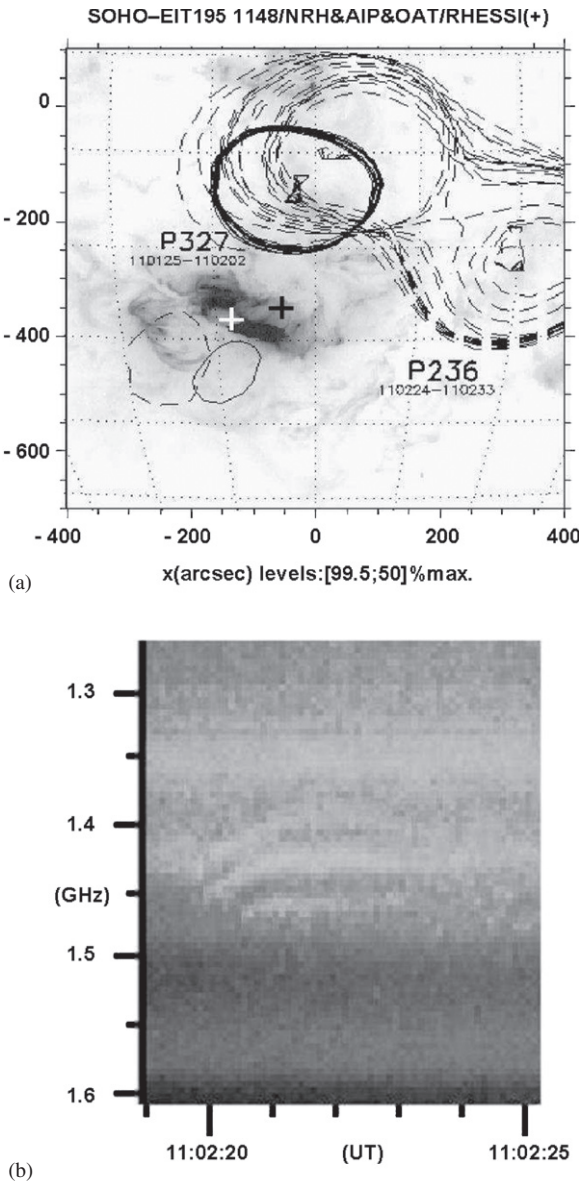

Figure 5. Radio source centroid transition from P1 to P2: (a) a *SOHO*-EIT 195 Å flare image with stacked NRH source positions of P1 (P327 at NRH 327 MHz, continuous isolines) showing one dominant source north of AR 10486. The source P2 (P236 at NRH 236.6 MHz, dashed) is split into two different sources near ARs 10491 and 10489 (compare Figure 1). The "+" signs mark *RHESSI* HXR flare sources. (b) In the break between P1 and P2 at meter waves, these three faint zebra stripes are observed in AOO spectra. Horizontal lanes are background in that image.

[5] Zebra stripes are a fine structure in radio continua, e.g., Chernov (2010) and Zlotnik et al. (2009), sometimes also reported in microwaves.

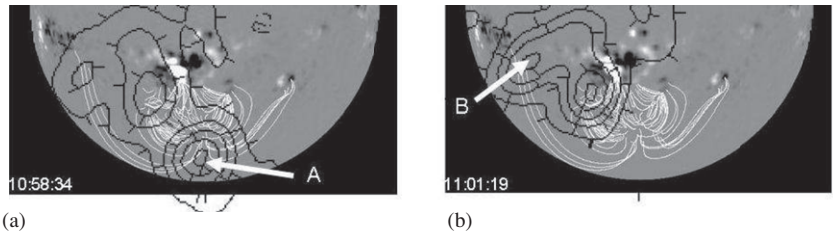

(a) (b)

Figure 6. On the same pfss-produced plot of potential field lines (*SOHO*-MDI; Schrijver & DeRosa 2003), the NRH 236.6 MHz isolines are drawn in the southeast quadrant, at the times of the faint radio features A (a) and B (b) of Figure 2.

236.6 MHz). Both sources are situated far off the flare center in AR 10486, which is marked by the HXR source centroids. We have stacked 95.5% and 50% isolines of all available images for the P1 and P2 time intervals on a *SOHO*-EIT map at 195 Å. Each image is normalized to its own maximum value. P1 coincides well with a remote source noticed to the north of AR 10486 in the main flare phase (Aurass et al. 2006). It is accompanied by a much fainter source (a quarter of the flux) southward of AR 10486 (see Figure 5(a), south of the white "+"). Significant pulsations can only be detected for the main source of P1.

We notice that the remote 327 MHz source site, which is identified as the main source of preflare pulsation P1 (Figure 2), was also the subject of our connectivity study (Aurass et al. 2007). This strong radio source is situated away from a photospheric magnetic field concentration, and we find no associated effects in any other spectral range. We explain this radio source as an effect of the field relaxation at the contact of separator field lines after CME liftoff and the flare maximum. The spatial coincidence of the preflare (P1) and main flare phase sources occurs with a time shift of 13 minutes, with the impulsive phase and the main flare phase onset in between.

Not only are the spectral signatures of P1 and P2 (Figure 2 and Figure 3) different but the source positions are as well. P2 corresponds with two displaced sources of about equal strength, and each subsource seems to belong to an active region: AR 10491 and 10489, respectively. This demonstrates that the disturbances evidenced by the sudden and oscillating rise of source P1 lead to a reaction in the entire surrounding coronal magnetic field in a neighboring (10491) but also in a more distant active region (see Figure 1).

Moreover, we observed just during the transition between P1 and P2 the zebra structure Z (Figures 2 and 5(b)). The spectrographically identified fine structure in dm radio emission cannot be imaged due to missing radioheliographs in this frequency range. However, referring to numerous case studies based on the spectrometer data of AOO (e.g., Karlický 2004), we can assume that dm fine structure sources are situated in the flaring active region 10486 and accompany the filament destabilization and eruption.

Summarizing, we draw the following speculative picture. A signal in the network of coronal QSLs, released by any small photospheric motion or magnetic field change, is the trigger disturbance for connectivity changes of field lines shielding AR 10486. Underneath this screen of field lines with an interconnecting length scale the eruptive instability of the highly sheared arcade has already been initiated (remember the decimeter DPS emission before P1 in Figure 2). After the connectivity changes the flux cells are slightly modified and the screen above AR 10486 is less stable against the sheared arcade. This is the signal for the liftoff of the filament.

Our hypothetical picture is strengthened by the following two important facts:

1. the synchronization of sources widely spaced in frequency (meter to decimeter) and in space (coronal magnetic field versus AR 10486 loops); and
2. the observation of the decimetric zebra pattern in the seconds between the occurrences of widely displaced meter wave sources P1 and P2. This indicates an accurately coinciding tiny heating/electron acceleration phenomenon within the flaring AR 10486.

In the NRH images, the minor radio bursts A and B also have widespread source sites away from active regions. We now compare the isolines of the A- and B-source maximum flux images with pfss-derived potential field line plots. First, we consider the field lines starting around the centroid of source A. It is situated on a line sharply dividing flux systems connected toward east and west (Figure 6(a)). Without a detailed analysis, we claim, based on this field line arrangement, that this source is associated with a QSL. Note that some field lines also connect site A with AR 10486 and that feature A in Figure 2 occurs simultaneously with the onset of the decimeter radio emission.

In Figure 6(b), we have drawn the radio image of burst B, which starts with the P1 onset. Some of the interconnecting field lines in Figure 6 span between source sites A and B.

Figure 7 shows a field line set anchored around centroid B (drawn in black), and combined with a field line set starting at the centroid of P1 (white). In this image, it is easy to find field lines connecting source site B with different positions south of AR 10486. Seen from B, however, there is a sharp separation between the black and white systems of field lines along the dashed black line inserted on the white background. In other words, there could be a QSL between both flux systems along this dashed line. Some of the white field lines with footpoints close to radio source P1 are associated with the null point (analyzed by Aurass et al. 2007) located at the north of AR 10486.

In Figure 3, several peaks are evident at 237 MHz with about a 20 s quasi-period between 11:01:15 and 11:02:30 UT. The smooth background source is situated south of AR 10486 and grows at the same time. We can doubtless identify some of the faint peaks as coming from short-lived sources occurring here and there along a line from source B moving northwest. This tendency is reproduced by the isolines in Figure 6(b) stretched from B in that direction. In Figure 7, the dotted white line denotes the short-lived narrowband meter wave source sites. We conclude that the flashing meter wave sources at and to the northwest of source B denote reconnection at several locations at the aforementioned inclined QSL, dividing the magnetic flux cells drawn in black and white in Figure 7.

3. DISCUSSION

The essence of Section 2 consists of evidence for the spatial association of faint meter wave preflare radio sources with

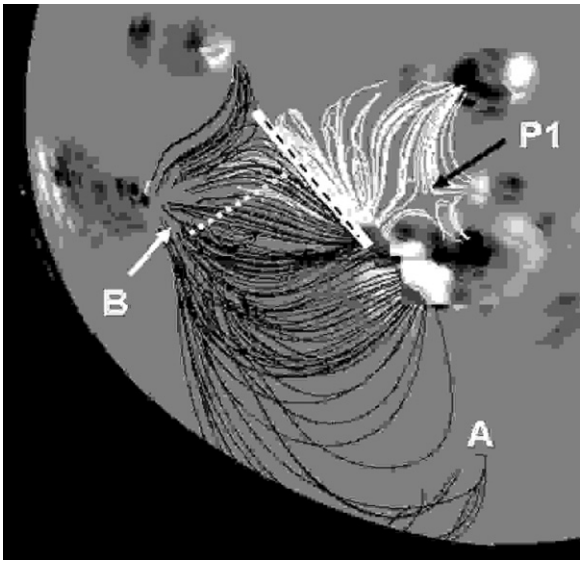

Figure 7. Composed picture of two different subsets of potential field lines based on the pfss (*SOHO*-MDI; Schrijver & DeRosa 2003). Black field lines start near the centroids around source site B. White field lines start near the centroid of P1. Some eastward extended lines of the white system spread underneath the dashed line. The spiky 236.6 MHz preflare sources (11:01:15–11:02:30 UT, at 237 MHz in Figure 3) which are distributed along the dotted line.

topologically sensitive regions in the large-scale coronal potential magnetic field around AR 10486 during the well-known halo-CME and X17 flare on 2003 October 28. We found different meter wave sources well synchronized with the evolution of decimeter flare burst sources immediately associated with processes under the filament in AR 10486.

Our analysis is focused on the time interval lasting from the earliest decimeter flare effect and the first faint meter wave signal (10:58:30 UT) to the impulsive phase start (≈11:02:30 UT) and the relation of these signals to the structure of the surrounding large-scale potential field.[6] The m-wave preflare emission is concentrated between 200 and 350 MHz. For a slightly enhanced Newkirk model density[7], this corresponds to a height range from some Mm up to ⩽80 Mm and seems to be an optimum range for the onset of the coronal energy release (Spicer 1977; Aurass et al. 2010). Our investigation fills the time gap between the works of Mandrini et al. (2006), which analyzes the energy storage and magnetic field structure in AR 10486 and the events occurring before 10:58:30 UT, and Pick et al. (2005), which considers effects after 11:02:30 UT.

In two earlier studies, Aurass et al. (2006) and Rausche et al. (2007) analyzed radio burst sources propagating along potential field structures from the flaring active region to several of the surrounding active regions. These bursts are denoted as "fiber burst" fine structure in dynamic spectra. They are relatively well understood in terms of a whistler wave model (Kuijpers 1975; Mann et al. 1987, 1989; Benz & Mann 1998). Analysis of the fiber burst sources revealed that a huge area around AR 10486 was still disturbed well after the CME release and the flare maximum. In a detailed connectivity analysis, we found a region of low photospheric longitudinal field at the source centroid of a strong radio continuum. We concluded that there could be a topologically determined acceleration site north of (this means away from) the flaring active region, and also away from other active regions (Aurass et al. 2007) coupled with the whistler wave excitation along large interconnecting field lines.

In the preflare phase of the event, we found a synchronized sequence of radio bursts distributed over a broad frequency range (here 0.2–4 GHz). Several narrowband (<100 MHz) sources are the more interesting ones: one occurring at 327 MHz as source P and reoccurring in the main flare phase (see Rausche et al. 2007, Figure 3), and several different 236.6 MHz source sites (A, B, P2) well timed with the decimeter emission in the preflare phase. By its repeated occurrence in the preflare as well as in the main flare phase, the 327 MHz source provides evidence that accelerated electrons are at disposal at a disturbed but stable site in the coronal potential magnetic field—at the converging separator field line configuration characterized in Aurass et al. (2007). This configuration points to the aforementioned low field region marked by the asterisk in Figure 1.

Remarkably, the OAT polarimeter record reveals a change in the polarization sense of this source in the main flare phase. The underlying continuum is initially R-polarized (4% R 11:10–11:13), unpolarized at 11:13:40, 4% L at 11:14:10, and 64% L after the saturation. During the strong growth of the source (at the same site where we found P1, 70% R-polarized before the impulsive phase) the sense of circular polarization is changed and rises further with time. We consider this as an independent and additional argument for the hypothesis that the radio source site, as well as the excitation and propagation of radio emission near the source volume, is sensitively connected with the magnetic field structure in and around the source volume.

A visual inspection of the potential field structure in the surroundings of sources A and B suggests that these faint preflare radio sources are situated at flux cell boundaries (QSLs). This means that we found at least three different sites on the disk, A, B, and P1, which are widely spaced around the flaring AR 10486, that flash up within 5 minutes before the broadband growth of the radio flux to the proper impulsive flare. Furthermore, we found two spatially different oscillating radio sources away from the flaring active region within 1.5 minutes before the huge eruption, the first at higher and the second at lower density, with pulsation periods of roughly 1 s and 0.5 s, respectively.

This means that the oscillations observed in the radio sources situated in field structures outside the flaring AR 10486 became faster with the approaching eruption. The transition between the oscillating meter wave sources is coupled with the occurrence of three distinct zebra stripes at ≈1.42 GHz. This fine structure, with a small number of stripes, and at high frequencies, is explained—for sources in the microwave range—by the occurrence of Bernstein modes in the source volume (Kuznetsov 2005). This plasma wave mode excites escaping gyroharmonics and occurs in the case of a highly anisotropic electron temperature in the magnetized source plasma (e.g., Treumann & Baumjohann 1997). Here, we have observations in the decimeter wave range, with a ratio of stripe distance to observing frequency of 1/7. At OAT, from 1.42 GHz polarimeter data, a polarization degree of 11%–13% R (almost the same as the background emission) was derived. The slightly polarized stripe emission has the same circular polarization sense as the preflare sources at lower frequencies for which we invoked the ordinary sense of polarization by simply referring to the escape conditions of the electromagnetic modes. This is in contrast with Kuznetsov's (2005) reporting of 100% extraordinary polarization at about 5 GHz.

[6] Obtained by extrapolation of the photospheric longitudinal field into the corona.

[7] We used 1.6 fold Newkirk (1961) as found for microflare sources (Aurass et al. 2010).

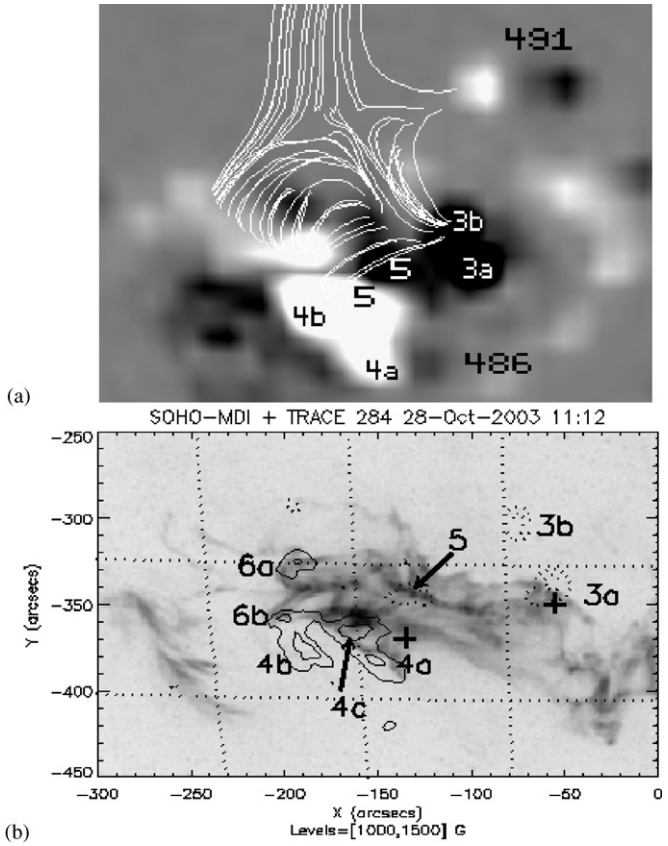

Figure 8. (a) pfss-plotted randomly selected field lines of the potential field with starting points near the magnetic field zero (asterisk in Figure 1) and the very northern part of the active region. For the notation see panel (b). Note the lines connecting the zero with spot 3b, and the linkage between spots 3b and 4b. (b) AR NOAA 10486 as seen by *TRACE* (284 Å) with superposed *SOHO*-MDI isolines (see Figure 1). Plus signs are the *RHESSI* HXR source centroids. The notions are (partly) according to Mandrini et al. (2006, Figure 3). Note that 3b and 4b are not covered by EUV signatures.

Nevertheless, given the low number of stripes, we accept his model for our observation. We should mention that the polarization sense of radio emission from a current sheet (probably sources A, B, and P1) is not obvious without detailed knowledge of geometry and viewing angle (Zheleznyakov 1996).

In Section 2, we were faced with the problem of missing decimeter imaging for the analyzed event. Based on the aforementioned theoretical and observational work at AOO (e.g., Karlický 2004), and the reported single event observations with, e.g., RATAN-600, Owens Valley, and the Very Large Array (e.g., Vourlidas et al. 1997), we assume that the whole decimeter emission in Figure 2 has source sites within the flaring active region. The meter wave imaging of the synchronized remote faint preflare features is perhaps unique and quite evident in the case of the very strong event considered.

The magnetic break-out model of CME initiation is based on a sheared quadrupolar magnetic configuration situated underneath a zero of the coronal magnetic field. At the zero, a minor reconnection process can initiate the following two consequences:

1. restructuring of the surrounding large-scale coronal field (possibly indicated by radio emission at the zero and at remote QSLs); and
2. the release of the shear leading to filament eruption, flaring, and CME formation in the active region.

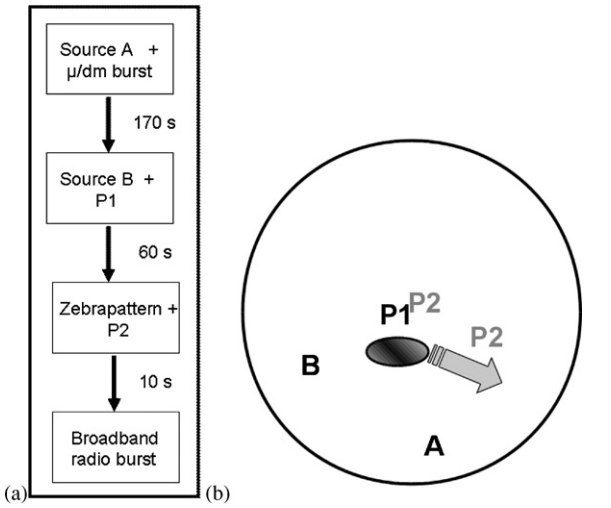

Figure 9. (a) Timeline of events in the stage before growth to the strong impulsive X17 flare phase. The start time is 10:58:30 UT. (b) The arrangement of the radio source sites on the disk around AR 10486 (the ellipse; not to scale). The arrow denotes later radio source centroids and plasma motions evolving in between 11:02:30 and 11:06:30 UT (Pick et al. 2005; Aurass et al. 2006).

We have observed all consequences in a correlated manner. The zero with radio emission, however, is far to the north of the flaring active region. So, how accurately can our observation be compared with this model?

For an answer we consider Figure 8. Here a pfss plot of the magnetic connectivity of the southern part of Figure 1 can be compared with a flare image of the corona (*TRACE* 284 Å 11:12 UT) with superposed strongest magnetic flux concentrations of a preflare magnetogram. Black polarity in panel (a) is dotted in panel (b), and white corresponds to continuous isolines. At the top the active region numbers are inserted. In both parts of the figure, we adopted the notion of the analysis of Mandrini et al. (2006, their Figure 3). The notion is slightly modified based on the potential field line connections in Figure 8(a). Using Mandrini et al. (2006, their Figure 5, top panel) as part of the preflare configuration there is a highly sheared set of field lines connecting flux concentration 3a with 6a and 6b. On a smaller scale, there is a connection 5–4c. The field concentrations 3b and 4b are not involved in flaring but are magnetically connected above the structures already described (see the *TRACE* image).

From *RHESSI* HXR source centroids, we know that the postflare loops are rooted in 3a and 4a. Thus, the quadrupolar sheared configuration consists of polarities (3a; 5) versus (4a+4c; 6). The low field region north of AR 10486 in Figure 8(a) (the magnetic zero) is magnetically connected to flux concentration 3b, which is also connected with 4b. Therefore, a disturbance at the zero (even if it is not situated on top of the quadrupolar configuration) can be guided to a field connection extending across the sheared preflare configuration, thus influencing the tension above the sheared configuration. The observed synchronization of the different effects and the repeated occurrence of radio emission from a source site near the magnetic zero support that possibility.

Figure 9 schematically summarizes the synchronization, time sequence, and spatial arrangement of the different sources. A bold arrow denotes the location where flare radio source centroids at NRH (observing frequencies $\leqslant$327 MHz) and mass motions, as well as postflare loops and CME tail patterns, were later observed (Pick et al. 2005; Aurass et al. 2006). The

flare-associated halo-CME starts according to the back extrapolation at 11 UT (see Table 1). Consequently, our interpretation of the observed chain of events is that the faint radio sources A and B, and at least the pulsating component of the source P1, are fed by nonthermal electrons accelerated during reconnection on QSLs between different magnetic flux systems. The radio sources are not accompanied by emission in other spectral ranges.

The sources of decimetric emission (with smooth spectral extensions into the microwave range not shown in Figure 2)—the dm burst start, the DPS features, the zebra stripes, and of course, the growth of the main flare burst—are radio signatures excited by particles accelerated during the energy release of the sheared preflare arcade in AR 10486 (meaning as a result of the proper flare process). The zebra stripes are in favor of a small-scale sudden anisotropic heating event somewhere in the flare plasma. If not by mere coincidence, the occurrence of this small-scale process in the active region together with the transition from P1 to P2 reveals that the connection between the large-scale coronal field and the flaring loops in the active region is still essential immediately before the impulsive flaring.

4. CONCLUSION

The described occurrence and synchronization of distributed meter wave radio sources with the development of the filament-associated "compact" decimeter flare sources in AR 10486 correspond with predicted radio phenomena in the magnetic break-out model of CMEs by Antiochos et al. (1999). We have demonstrated how, in regions of low coronal magnetic field between different coronal flux cells (QSLs), widely distributed small-scale processes revealed by radio emission of minor amounts of nonthermal electrons indicate the disturbance of the large-scale corona. Further, we have shown how a low field region of the observed longitudinal photospheric magnetic field (connected with converging separator field lines of three distinct flux cells; Aurass et al. 2007) coincides with the centroid of a pulsating radio source about 70 s before the broadband radio burst of the X-class flare. The pulsation period is 1 s, while the duration of the pulse train is about 30 s. The potential field extrapolation of the Michelson Doppler Imager (MDI) observations (Schrijver & DeRosa 2003) reveals that the pulsating radio source site near the low field region is magnetically connected with the northern footpoint of a field connection across the active region, which is not directly involved in flaring but situated above the sheared preflare structure in the active region.

This means our observations do not directly coincide with the configuration considered for the break-out model of a CME. The magnetic zero and the associated radio emission are not situated above but north of the flaring quadrupolar magnetic field region. However, we could demonstrate that the magnetic zero north of AR 10486 is connected with a flux system that bridges the flaring region. So, we do not exclude the notion that reconnection at the zero influences the magnetic tension on top of the sheared preflare structure as happens in the case of the break-out model.

The revival of the former pulsating source in the form of a strong postflare continuum source at the same site and in the presence of whistler wave-driven radio spectral fine structures (fibers) at interconnecting magnetic field lines serves as support to our understanding of the data. We argue that the remarkable frequency of occurrence of whistler waves (Aurass et al. 2006) is a sign of the relaxation of the disturbed corona back to its quiescent state after the release of the CME. A change of the polarization sign of the strong 327 MHz source strengthens the interpretation, but could also be induced by a different viewing angle.

This work is not the first paper describing observations of relevance for the magnetic break-out model of CMEs (see, for instance, Gary & Moore 2004; Mandrini et al. 2006; Lin et al. 2010). It is, however, based on a heretofore unique data set, the first report on faint and distributed coronal radio sources, correlated in detail with the dm burst evolution from inside the flaring active region, and their relation to the flux cell structure of the large-scale potential magnetic field. Therefore we also consider what the potential field can tell us about the magnetic linkage between a radio-detected low-field region and several radio sources at QSLs with the flaring quadrupolar structure in AR 10486. We hope that the observations presented support further discussion between observers and theorists about models of flare and CME initiation.

We acknowledge the open access to the Nançay Multifrequency Radioheliograph data and are grateful to the team supporting regular observations with this instrument. Further, we acknowledge the use of *SOHO*-MDI and EIT, as well as *TRACE*, *RHESSI*, and *GOES* data. *SOHO* is a common space mission of ESA and NASA. The work of H.A. was kindly supported by Grant DFG (Deutsche Forschungsgemeinschaft) AU 106/13-2. H.A. acknowledges discussions with P. Démoulin during the COSPAR2010 meeting. Thanks are due to the anonymous referee whose careful reading and constructive criticism essentially improved the presentation of this manuscript.

REFERENCES

Antiochos, S. K., DeVore, C. R., & Klimchuk, J. A. 1999, ApJ, 510, 485
Antiochos, S. K., Karpen, J. T., & DeVore, C. R. 2002, ApJ, 575, 578
Aurass, H., Mann, G., Rausche, G., & Warmuth, A. 2006, A&A, 457, 681
Aurass, H., Rausche, G., Berkebile-Stoiser, S., & Veronig, A. 2010, A&A, 515, A1
Aurass, H., Rausche, G., & Mann, G. 2007, A&A, 471, L37
Barta, M., Karlický, M., & Žemlička, R. 2008, Sol. Phys., 253, 173
Benz, A. O., & Mann, G. 1998, A&A, 333, 1034
Chen, J. 1989, ApJ, 338, 453
Chernov, G. P. 2010, Rev. Astron. Astrophys., 10, 821
Démoulin, P., Hénoux, J. C., Priest, E. R., & Mandrini, C. H. 1996, A&A, 308, 643
Fleck, B., Domingo, V., & Poland, A. (ed.) 1995, The SOHO Mission (Dordrecht: Kluwer)
Gary, G. A., & Moore, R. L. 2004, ApJ, 611, 545
Handy, B. N., et al. 1999, Sol. Phys., 187, 229
Hurford, G. J., Krucker, S., & Lin, R. P. 2006, ApJ, 644, L93
Jiřička, K., Karlický, M., Kepka, O., & Tlamicha, A. 1993, Sol. Phys., 147, 203
Karlický, M. 2004, A&A, 417, 325
Kerdraon, A., & Delouis, J. 1997, in LNP 483, ed. G. Trottet (Heidelberg: Springer), 192
Kiener, J., Gros, M., Tatischeff, V., & Weidenspointer, G. 2006, A&A, 445, 725
Klassen, A., Krucker, S., Kunow, H., Müller-Mellin, R., Wimmer-Schweingruber, R., Mann, G., & Posner, A. 2005, J. Geophys. Res., 110, A09S04
Kliem, B., & Török, T. 2006, Phys. Rev. Let., 96, 5002
Kuijpers, J. 1975, Sol. Phys., 44, 173
Kuznetsov, A. A. 2005, A&A, 438, 341
Lin, C. H., Gallagher, P. T., & Raftery, C. L. 2010, A&A, 516, 44L
Lin, R. P., et al. 2002, Sol. Phys., 210, 3
Lynch, B. J., Antiochos, S. K., DeVore, C. R., Luhmann, J. G., & Zurbuchen, T. H. 2008, ApJ, 683, 1192
MacNeice, P. J., Antiochos, S. K., Phillips, A., Spicer, D. S., DeVore, C.R., & Olson, K. 2004, ApJ, 614, 1028
Magdalenič, J., Zlobec, P., Messerotti, M., & Vršnak, B. 2002, Proc. 10th ESP Meeting, Prague, 331
Mandrini, C. H., Démoulin, P., Schmieder, B., Deluca, E. E., Pariat, E., & Uddin, W. 2006, Sol. Phys., 238, 293

Mann, G., Aurass, H., Voigt, W., & Paschke, J. 1992, Coronal Streamers, Coronal Loops, and Coronal and Solar Wind Composition (ESA SP-348; Noordwijk: ESA), 129
Mann, G., Baumgärtel, K., Chernov, G. P., & Karlický, M. 1989, Sol. Phys., 120, 383
Mann, G., Karlický, M., & Motschmann, U. 1987, Sol. Phys., 110, 381
Newkirk, G. A. 1961, ApJ, 133, 983
Pick, M., Malherbe, J.-M., & Kerdraon, A. 2005, ApJ, 631, L97
Priest, E. R., & Démoulin, P. 1995, J. Geophys. Res., 100, 23443
Priest, E. R., & Forbes, T. G. 2000, Magnetic Reconnection (Cambridge: Cambridge Univ. Press)
Rausche, G., Aurass, H., Mann, G., Karlický, M., & Vocks, C. 2007, Sol. Phys., 245, 327
Reiner, M. J., Karlický, M., Jiřička, K., Aurass, H., Mann, G., & Kaiser, M. L. 2000, ApJ, 530, 1049
Schrijver, C. J., & DeRosa, M. L. 2003, Sol. Phys., 212, 165
Somov, B. V. 1986, A&A, 163, 210
Somov, B. V. 2000, Cosmic Plasma Physics (Dordrecht: Kluwer)
Spicer, D. S. 1977, Sol. Phys., 53, 305
Treumann, R., & Baumjohann, W. 1997, Advanced Space Plasma Physics (London: Imperial College Press)
Trottet, G., Krucker, S., Lüthi, T., & Magun, A. 2008, ApJ, 678, 509
Vourlidas, A., Bastian, T. S., & Aschwanden, M. J. 1997, ApJ, 489, 403
Zheleznyakov, V. V. 1996, Radiation in Astrophysical Plasmas (Dordrecht: Kluwer)
Zlotnik, E. Ya., & Sher, É. M. 2009, Radiophys. Quantum Electron., 52, 88